STUDY ON ANTI-EXPLOSION BEHAVIOR
OF HIGH-STRENGTH REINFORCED CONCRETE BEAM
UNDER BLAST LOADING

Z. Liao,[a] **Z. Z. Li,**[a,1] **Y. L. Xue,**[b,2] **L. Z. Shao,**[a]   UDC 539.4
D. P. Yang,[a,c] **and D. G. Tang**[a,3]

To investigate the anti-explosion behavior of high-strength reinforced concrete (RC) beam subjected to blast load, the ANSYS/LS-DYNA finite element analysis software was applied. Based on anti-explosion test results, the effects of reinforcement strength grade, reinforcement ratio and stirrup ratio on dynamic response, failure mode, resistance curve and ductility of RC beams under uniform blast load were studied. The anti-explosion performance of RC beam can be effectively improved by increasing the strength grade of the high-strength reinforcement. When the shear capacity is high enough, the ultimate capacity of high-strength RC beam can be significantly enhanced by increasing its reinforcement ratio. Anti-explosion performance may deteriorate due to the change of failure modes when the reinforcement ratio is increased to a certain extent. Increasing stirrup ratio can improve the shear capacity of high-strength RC beam to guarantee the full utilization of the advantage of high flexural capacity. For high-strength RC beam with sufficiently shear capacity, the further increase of stirrup ratio has a slight effect on the anti-explosion ability.

Keywords: blast load, high-strength reinforced concrete beam, anti-explosion behavior, numerical simulation.

Introduction. The rapid development of modern strike weapons has put forward higher requirements for the anti-damage ability of protective engineering structures, including high-strength reinforced concrete (RC) ones. In recent years, a series of research work on the dynamic response of reinforced concrete structures under blast load was performed worldwide [1, 2]. For example, Kuang et al. [3] carried out an experimental study on ordinary RC beams with the HRB335 tensile reinforcement under blast load and analyzed the variation of crack propagation, strain, and deflection of the beams under different blast loads. Chen et al. [4] carried out the anti-explosion performance test of high-strength RC slabs with the HTB600 reinforcement and analyzed the influence of reinforcement ratio, concrete strength grade, section dimension, and other factors on the anti-explosion capacity of high-strength RC slabs. Li et al. [5] studied the characteristics and mechanism of damage and failure of RC beams with the HRB400 tensile reinforcement by using explosion pressure simulator and carried out the numerical simulation of the whole process of deformation and failure under blast load. Yao et al. [6] used the LS-DYNA finite element software to analyze the failure modes of RC beams with the HPB235 tensile reinforcement, which yielded the deflection formulas of ordinary RC beams subjected to blast loads. Yoo et al. [7] used a drop-hammer test device to assess the dynamic

[a]State Key Laboratory for Disaster Prevention & Mitigation of Explosion & Impact, Army Engineering University of PLA, Nanjing, Jiangsu, China ([1]lizz0607@163.com; [3]tgd6206@163.com). [b]Research Institute for National Defense Engineering of Academy of Military Science PLA, Beijing, China ([2]karl_xue88@outlook.com). [c]Research Institute for National Defense Engineering of Academy of Military Science PLA, Luoyang, Henan, China.

response of fiber-reinforced concrete beams subjected to impact load and revealed the effect of reinforcement ratio on their flexural bearing capacity. Mao and Barnett [8] adopted the combination of experimental study and numerical calculation to study the dynamic response of fiber-reinforced concrete beams subjected to different impact loads and the derived relationship between their impact resistance and the loading rate.

It can be seen from the above survey that most of the research results on anti-explosion performance of RC structures at present have been made on reinforced concrete structures with ordinary strength reinforcements [9–12]. The yield strength of reinforcement usually did not exceed 400 MPa, and there was little research on the anti-explosion performance of RC structures with high-strength reinforcements. High-strength construction steel bars combine high strength and large plasticity, which ensure their broad application prospects in military and civil structures.

In this paper, the dynamic response of high-strength RC beams subjected to blast loading is simulated by using the general finite element-based LS-DYNA software, and the simulation results are compared with the experimental ones to verify the reliability of the numerical calculation method and material parameters. On this basis, the anti-explosion performance of high-strength RC beams is further analyzed, and the effects of reinforcement strength grade, reinforcement ratio, and stirrup ratio on the dynamic response, failure mode, resistance curve, and ductility of high-strength RC beams are conducted, which may provide reference for the application of high-strength RC beams in the field of civil and military engineering protection structures.

1. Numerical Analysis of Anti-Explosion Performance Test. As a basic research method, the numerical simulation is widely used in the field of structural anti-explosion performance. To provide a basis for further analysis of the influencing factors of high-strength RC beams, the experimental results of explosion tests with peak overpressure of 0.477 MPa (where HB3-1 and HB3-2 correspond to the ordinary and high-strength RC beams, respectively) in [13] have been used in this study. The longitudinal reinforcement of the HB3-1 beam was HRB400, while the longitudinal reinforcement of the HB3-2 beam was HTB700. HRB400 is the abbreviation for hot-rolled ribbed bars with standard yield strength of 400 MPa, while HTB700 refers to hot-rolled ribbed bars with the yield strength standard value of 700 MPa. The general finite element analysis ANSYS/LS-DYNA software was used to carry out numerical simulations, which results were experimentally validated to verify the numerical calculation model and calculation parameters.

1.1. Material Model.

1.1.1. Concrete. Concrete under blast load is exposed to large strains, high confining pressures, and high strain rates. The keyword *MAT_CONCRETE_ DAMAGE_REL3 provided by LS-DYNA was adopted to better reflect the mechanical response and deformation characteristics of concrete under strong impact blast load. This model only requires users to input several parameters, such as elastic modulus and axial compressive strength of concrete, while other material parameters are automatically generated by the model [14–17].

The strength index of concrete under blast load has significant rate dependent characteristics [18, 19]. The material model considers the characteristics of concrete by inputting a user-defined strain rate enhanced coefficient curve. The European Code (CEB-FIP) [20] proposed a calculation model of concrete rate-dependent characteristics based on a large number of experimental data. The concrete strength grade used in the test was C40 and the concrete compressive strength of RC beams was 36.0 MPa [13]. According to the calculation formula of CEB-FIP [20], the strength enhancement coefficient curve is shown in Fig. 1. CDIF and TDIF are the compressive strength and tensile strength enhancement coefficient curve of concrete, respectively.

1.1.2. Reinforcement. Keyword *MAT_PLASTIC_KINEMATIC provided by LS-DYNA was used in this paper as considering the stress and deformation characteristics of reinforcement under blast load. The model is a hybrid model of isotropic and kinematic hardenings related to strain rate and failure. This model can consider the strain rate effect and failure of materials [17]. The strain rate effect of reinforcement is considered by using the Cowper–Symonds model [21], and the dynamic yield strength of reinforcement is calculated, according to the following formula:

$$\sigma_y = \left[1 + \left(\frac{\dot{\varepsilon}}{C} \right)^{1/P} \right] (\sigma_0 + \beta E_p \varepsilon_p^{eff}), \tag{1}$$

TABLE 1. Material Parameters of the Finite Element Model of RC Beams

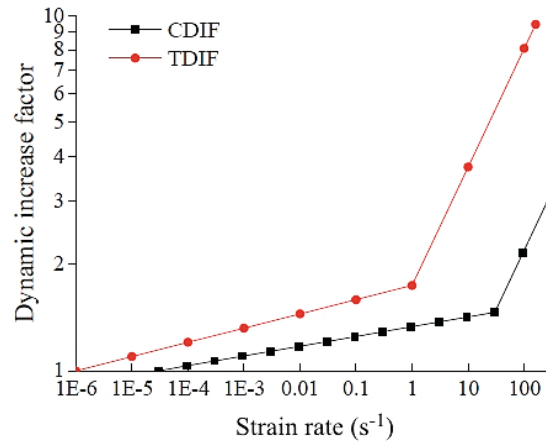| Material	Density (kg/m³)	Poisson's ratio	Elastic modulus (GPa)	Axial compressive strength (MPa)	Yield strength (MPa)
Concrete	2500	0.2	–	36.0	–
HRB400	7800	0.3	200	–	400
HTB700	7800	0.3	200	–	700
HTB900	7800	0.3	200	–	900
Support	7800	0.3	200	–	–

Fig. 1. Strength enhancement coefficient curve of test beam concrete.

where σ_y is the dynamic yield stress, σ_0 is the initial yield stress, $\dot{\varepsilon}$ is the strain rate, C and P are the strain rate parameters, ε_p^{eff} is the effective plastic strain, β is the hardening parameter, and E_p is the plastic modulus.

1.1.3. Support. Since the support used in the test was a steel support fixed to the ground, the deformation during the test was small and could be regarded as a rigid body. The keyword *MAT_RIGID is used to define it. To avoid numerical calculation problems at the sliding contact surface, the model requires the input of the true elastic modulus and Poisson's ratio of the support material [21]. The main material parameters of the finite element model of RC beams established in this paper are shown in Table 1.

1.2. Finite Element Model. The anti-explosion performance tests were carried out in an explosion pressure simulator and the blast shock wave generated by detonating cord uniformly acted on the upper surface of the test beams. The principle and results of the tests are referred to literature [13]. The stirrup ratio was 0.38% with a diameter of 6 mm and an interval of 100 mm. The finite element model of the test beam was established by using the node-split reinforced concrete model, which means that there was no relative slip between steel bar and concrete. The dimensions of the RC beams and the support in the finite element model were exactly the same as those in the test. To improve the calculation efficiency and reduce the data storage volume, a 1/4 finite element model of RC beams was established by using symmetry as shown in Fig. 2, and the corresponding symmetrical constraint conditions were applied on the two symmetrical surfaces. Both the concrete and support adopted hexahedral solid elements (SOLID 164), while the reinforcement adopted three-node beam elements (BEAM 161). To determine a reasonable finite element mesh size, the grid size dependence of the numerical calculation results was analyzed. By comparing the calculation results of four kinds of mesh sizes (2.5, 2.0, 1.0, and 0.5 cm) and giving consideration to the calculation efficiency, the grid size selected in this paper was finally set at 1.0 cm. The measured overpressure time–history curves corresponding to test conditions were used as input load for numerical calculation, as shown in Fig. 3.

1.3. Comparative Analysis of Numerical and Experimental Results. Figure 4 shows the experimental results and the corresponding deformation nephogram of both RC beams. According to the color distribution in deformation nephogram, the crack development and failure degree of RC beam can be determined qualitatively. It
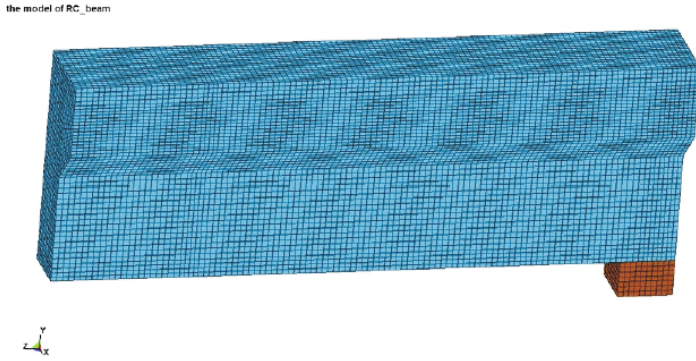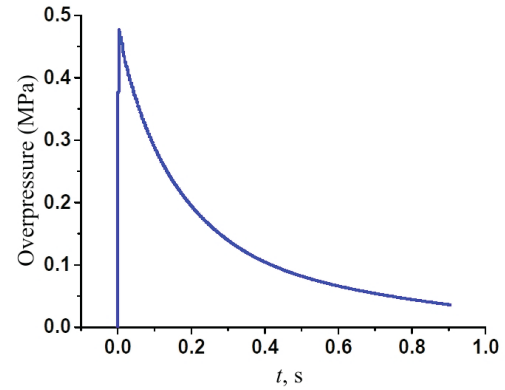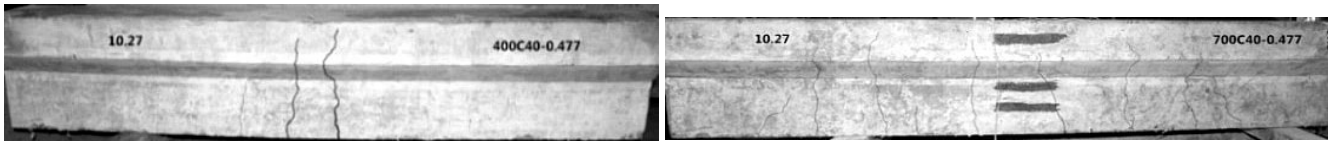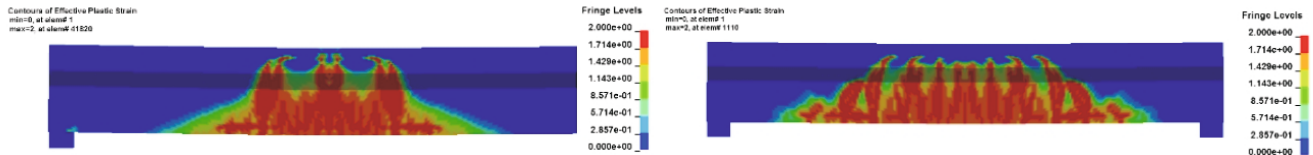
Fig. 2. 1/4 FE model of test beam.

Fig. 3. Measured overpressure time–history curve.

(a) Damage of beam HB3-1

(b) Damage of beam HB3-2

(c) Deformation nephogram of beam HB3-1

(d) Deformation nephogram of beam HB3-2

Fig. 4. Comparison of the deformation nephograms and the damage of test RC beams.

can be seen from Fig. 4 that the plastic damage area of ordinary RC beams (HB3-1) obtained by numerical calculation is slightly larger than the actual crack area, and that of high-strength RC beams (HB3-2) is basically consistent with the test results. The calculation results show that the damage near the mid-span of the ordinary RC beam extends almost to the top of the beam. The height of the damage zone of the high-strength RC beam is about 26 cm (the beam height is 30 cm), and the damage degree is obviously smaller than that of the ordinary RC beam. The numerical results are in good agreement with the crack distribution and failure degree of the test RC beams.

The numerical values and test values of the maximum mid-span displacement and maximum reinforcement strain of the two RC beams are shown in Table 2. It can be seen from Table 2 that the error between the numerical value and the test value of the mid-span maximum deflection is within 9.2%, and the error of the mid-span maximum reinforcement strain is within 2.2%.

From the above comparative analysis, it can be seen that the numerical calculation method and material parameters adopted in this paper can well simulate the dynamic response and failure characteristics of high-strength RC beams under blast load. It can be used to carry out the analysis of influencing factors on the anti-explosion performance of high-strength RC beams.

2. Influencing Factors Analysis of Anti-Explosion Behavior of High-Strength RC Beams.

2.1. Numerical Calculation Conditions. To further study the anti-explosion law of high-strength RC beam, the typical rectangular reinforced concrete beam was taken as the research object. The dimensions of the beam were $1700 \times 150 \times 300$ mm (length × width × height) with a net span of 1500 mm. The modeling method and the type of element were exactly the same as in Section 2.2. The RC beam was meshed with a grid size of 1.0 cm. The reinforcement was divided into 1,496 units, and the concrete and support were split into 77,952 and 900 units, respectively. The numerical calculation condition is shown in Table 3. The reinforcement strength grades corresponding to the three kinds of yield strength rebar were HRB400, HTB700, and HTB900, respectively.

TABLE 2. Comparison of Numerical and Test Results on RC Beams

Beam No.	Max. mid-span displacement (mm)			Max. mid-span reinforcement strain (10^{-6})		
	Test value	Numerical value	Error (%)	Test value	Numerical value	Error (%)
HB3-1	13.1	14.3	9.2	–	20583	–
HB3-2	11.8	10.9	7.6	4611	4520	2.0

Note: "–" means the value is not measured in the test.

TABLE 3. Numerical Calculation Condition

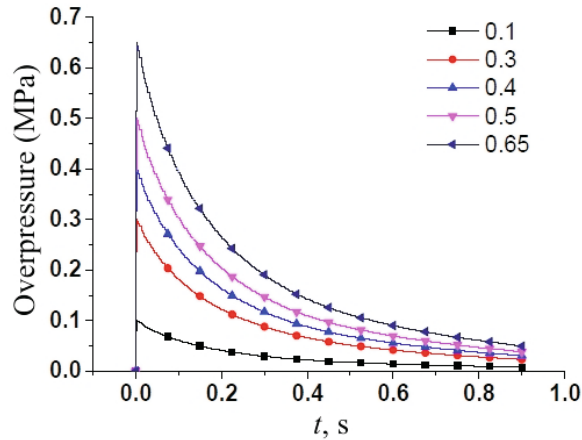| Reinforcement ratio (%)	0.25			0.40			0.57		
Yield strength (MPa)	400	700	900	400	700	900	400	700	900
Stirrup ratio (%)	0.67			0.67	0.38, 0.67, 1.05	0.67	0.67		

Fig. 5. Part of input load curves for numerical calculation.

2.2. Blast Load. The dynamic response and damage degree of the RC beam under different blast load are obtained by numerical calculation through applying the uniformly distributed blast load to the upper surface of the finite element model. The numerically calculated input load is determined from the measured explosion overpressure time–history curve. It can be seen from Fig. 3 that the measured overpressure time–history curve with a peak overpressure value of 0.477 MPa is exponentially attenuated, which is in accordance with the attenuation form of typical blast shock waves. In this paper, the overpressure time–history curve in Fig. 3 is taken as the basic load curve, and other load curves obtained by multiplying them by different coefficients are used as numerical input loads. Some of the input load curves for numerical calculation are shown in Fig. 5. To facilitate the comparative analysis, all calculation conditions are numbered, and the numbering format is "reinforcement ratio–yield strength of longitudinal reinforcement–peak overpressure of blast load."

2.3. Damage Nephograms of RC Beam. The concrete damage nephograms under different calculation conditions are used to compare the failure degree and characteristics of RC beams with different reinforcement ratios and different longitudinal reinforcement strengths, in order to obtain the deformation and failure process of RC beams.

2.3.1. Reinforcement Ratio of 0.25%. Figure 6 shows the concrete damage nephograms of three kinds of high-strength RC beams under different uniformly distributed blast loads at the reinforcement ratio of 0.25%.
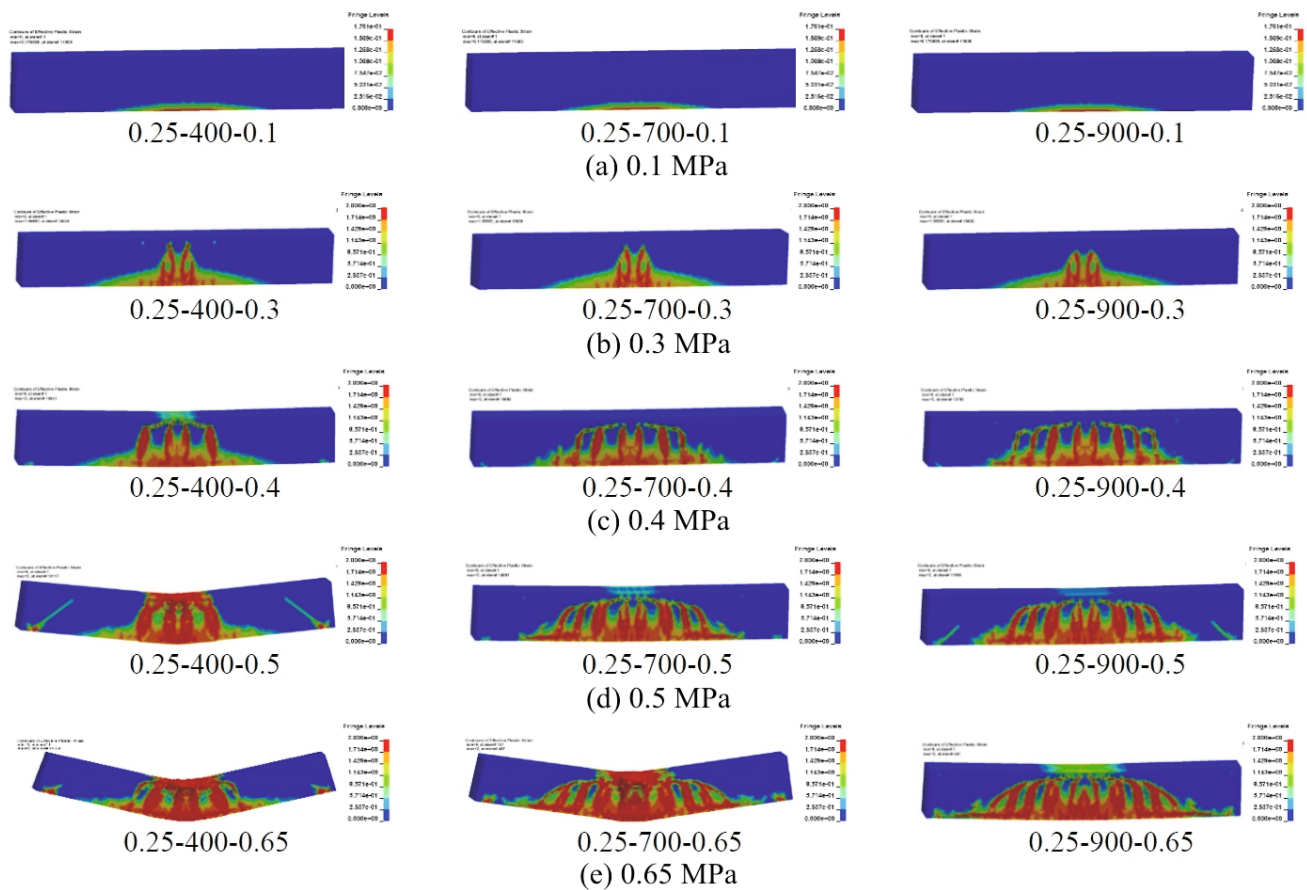
Fig. 6. Concrete damage nephograms of RC beams with reinforcement ratio of 0.25%.

It can be seen from the Fig. 6 that: (a) under the blast load of 0.1 MPa, only a small amount of concrete in the bottom tension zone of the three RC beams has plastic deformation; (b) when the blast load increases to 0.3 MPa, cracks are formed in the plastic area at the bottom near the mid-span of RC beams along the beam height, and the length of cracks gradually decreases with reinforcement strength; (c) when the blast load increases to 0.4 MPa, the number and length of cracks of the three RC beams increase to different extents. The top surface of HRB400 ordinary RC beam shows large plastic deformation, and its crack extends almost to the top surface of the beam, while the HTB700 and HTB900 high-strength RC beams have a large number of cracks and the crack height and damage degree are significantly smaller than the HRB400 ordinary RC beam, due to the occurrence of cracks effectively dissipating the blast wave energy; (d) when the blast load increases to 0.5 MPa, the concrete in the compression zone of the HRB400 ordinary RC beam is crushed, and the crack penetrates the entire mid-span section and forms a plastic hinge. At this time, a typical bending failure occurs. The crack distribution areas of the two high-strength RC beams continue to expand toward the ends of the support, and more cracks are formed. The concrete in the top compression zone shows a slight plastic deformation, but the RC beams undergo no bending failure; (e) when the load continues to increase to 0.65 MPa, the concrete in the compression zone of the HTB700 high-strength RC beam is crushed, and the crack runs through the entire mid-span section. The HTB700 high-strength RC beam shows typical bending failure. Although the concrete of the HTB900 high-strength RC beam in the compression zone is plastically deformed, there is no bending failure.

In summary, the deformation and failure degree of ordinary RC beam and high-strength RC beam are basically the same under small overpressure blast loads. With an increase in blast load, the number of cracks in high-strength RC beams is higher than that in ordinary RC beams, but the length of cracks and the damage degree of the beams are obviously reduced. All three RC beams ultimately suffer from bending failure.
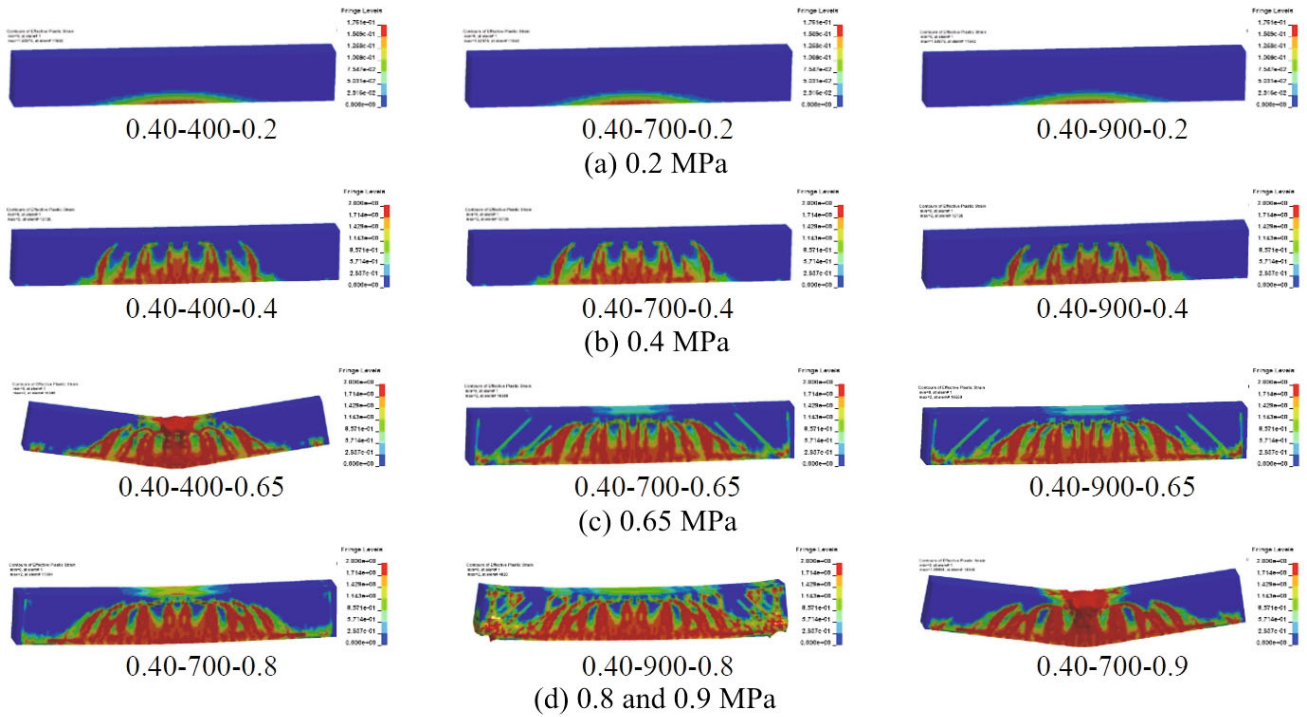
0.40-400-0.2	0.40-700-0.2	0.40-900-0.2

(a) 0.2 MPa

0.40-400-0.4	0.40-700-0.4	0.40-900-0.4

(b) 0.4 MPa

0.40-400-0.65	0.40-700-0.65	0.40-900-0.65

(c) 0.65 MPa

0.40-700-0.8	0.40-900-0.8	0.40-700-0.9

(d) 0.8 and 0.9 MPa

Fig. 7. Concrete damage nephograms of RC beams with reinforcement ratio of 0.40%.

2.3.2. Reinforcement Ratio of 0.40%. The concrete damage nephograms of three kinds of high-strength RC beams under different uniformly distributed blast loads when the reinforcement ratio is 0.40% as shown in Fig. 7.

It can be seen from Fig. 7 that: (a) when the blast load increases from 0.2 to 0.4 MPa, the crack distribution and damage degree of the three RC beams are basically the same; (b) when the explosive load increases to 0.65 MPa, a plastic hinge is formed in the mid-span of an ordinary RC beam, and a typical bending failure occurs. Two kinds of high-strength RC beams have slight plastic deformation at the top of the compression zone. The damage range of the concrete is larger than that of the ordinary RC beams, but there is no failure; (c) when the blast load reaches 0.8 MPa, the concrete at the top of HTB700 high-strength RC beam shows a large plastic deformation, and the crack extends along the beam height direction. At this time, the HTB700 high-strength RC beam is not destroyed. The crack area of HTB900 high-strength RC beam expands toward the support at both ends, and direct shear cracks occur near the supports, resulting in direct shear failure. This is because the yield strength of the longitudinal reinforcement is too high, making the shear bearing capacity of the beam less than the flexural bearing capacity and, finally, a shear crack is formed under the shear action near the support; (d) when the explosive load increases to 0.9 MPa, the middle section of HTB700 high-strength RC beam appears to penetrate due to the crack development, and the concrete in the compression zone is crushed, which results in a typical bending failure.

2.3.3. Reinforcement Ratio of 0.57%. The concrete damage nephograms of three kinds of high-strength RC beams under different uniformly distributed blast loads when the reinforcement ratio is 0.57% as shown in Fig. 8.

It can be seen from Fig. 8 that: (a) when the blast load increases from 0.4 to 0.6 MPa, the crack distribution and damage degree of ordinary RC beams and high-strength RC beams are basically the same, both of which show that the plastic damage area of concrete extends from mid-span to support and beam height as the blast load increases; (b) when the blast load increases to 0.8 MPa, the ordinary and high-strength RC beams begin to show different deformation characteristics. The width of the crack zone of the ordinary RC beam is basically unchanged. The deformation of the beam is concentrated in the formed plastic area in the span, and the concrete in the compression zone shows more serious plastic deformation. The cracked concrete area of high-strength RC beam expands towards the support; (c) when the blast load increases to 0.9 MPa, all three RC beams are damaged, but failure modes are obviously different. The ordinary RC beam has a plastic hinge in the mid-span section. However,

0.57-400-0.4 0.57-700-0.4 0.57-900-0.4

(a) 0.4 MPa

0.57-400-0.6 0.57-700-0.6 0.57-900-0.6

(b) 0.6 MPa

0.57-400-0.8 0.57-700-0.8 0.57-900-0.8

(c) 0.8 MPa
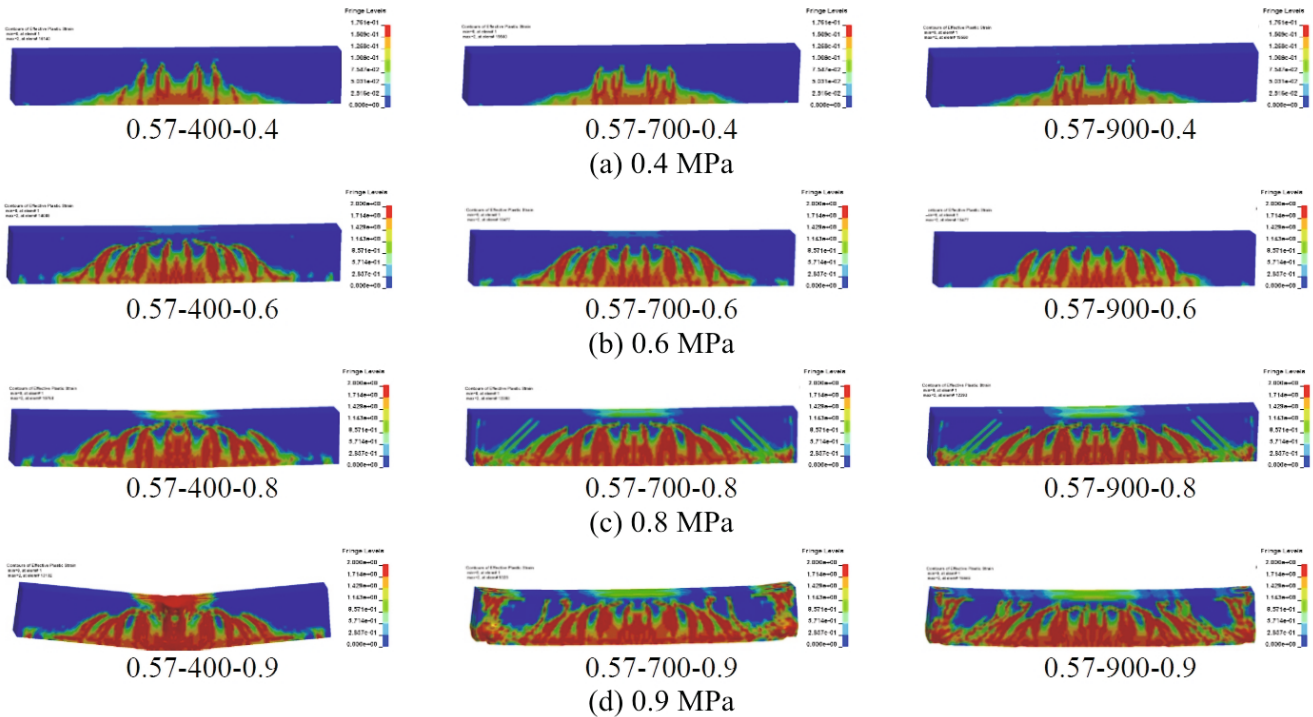
0.57-400-0.9 0.57-700-0.9 0.57-900-0.9

(d) 0.9 MPa

Fig. 8. Concrete damage nephograms of RC beams with reinforcement ratio of 0.57%.

after the HTB700 high-strength RC beam and the HTB900 high-strength RC beam form a direct shear crack at the support, the deformation is concentrated in the crack region near the support, and the high-strength RC beam eventually undergoes a direct shear failure.

In summary, when the reinforcement ratio is 0.57%, the deformation characteristics and damage degree of ordinary and high-strength RC beams are basically the same under small overpressure blast loads. With the increase of blast loading, the flexural capacity of high-strength RC beams is larger, but the actual anti-explosion ability is not improved compared with ordinary RC beams due to the direct shear failure.

2.4. Resistance Curve of RC Beam. The resistance curve of RC beams reflects the inherent mechanical properties of components, and is an important basis for carrying out accurate and reasonable dynamic analysis and design of protective engineering [22, 23]. The typical resistance curve of simply supported RC beam is shown in Fig. 9.

To analyze the dynamic and mechanical characteristics of the high-strength RC beam under the blast load, the resistance curve of RC beam is obtained according to the peak overpressure and the maximum mid-span displacement of the RC beam under different load conditions. The following resistance curve is described in the form of load–displacement curve.

2.4.1. Effect of Reinforcement Strength. To study the influence of the longitudinal reinforcement strength on the RC beam resistance curve, the influence of different longitudinal reinforcement strength values on the deformation characteristics and failure mode of the RC beam is analyzed. Figure 10 shows the load–displacement curves of RC beams with HRB400, HTB700, and HTB900 longitudinal reinforcements at the reinforcement ratio of 0.25%.

As can be seen from the diagram, the shape of the three curves is similar and there are two obvious turning points marked as *A* and *B* points. The resistance curves are divided into three sections by *A* and *B* points, which represent three different deformation stages of RC beam. The change of curve slope reflects the variation of bending stiffness of RC beams from cracking to failure. In the *OA* section, the three curves are completely coincident, and the peak overpressure value of the blast load is approximately linear with the mid-span displacement. This is because the elastic modulus of the high-strength reinforcement is the same as that of the ordinary reinforcement, so the
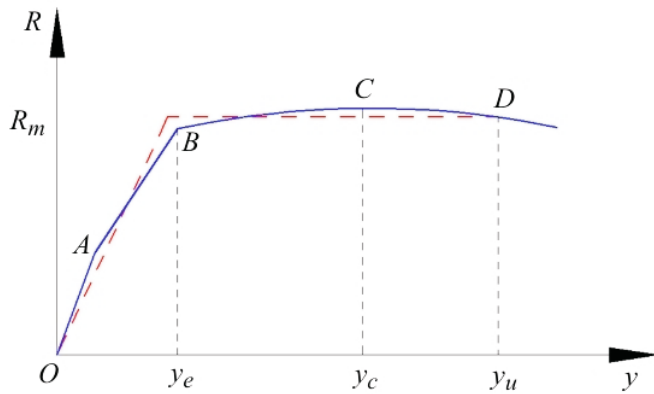
Fig. 9

Fig. 10

Fig. 9. Typical resistance curve of simply supported RC beam. (*A* – tensile zone concrete cracking, *B* – tensile reinforcement begins to yield, *C* – compression zone concrete crushing, *D* – obvious resistance reduction stage, and R_m is the maximum resistance of RC beam.)
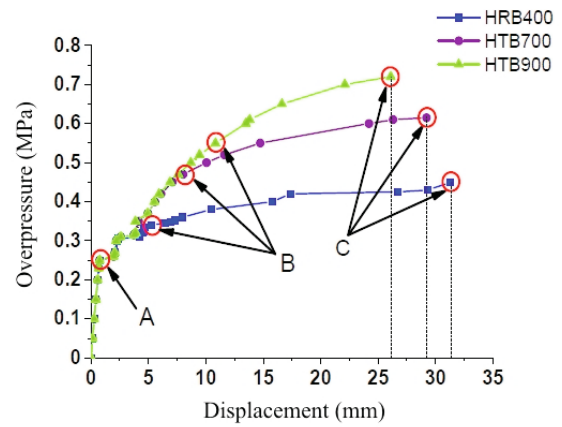
Fig. 10. Load–displacement curves of RC beams with different reinforcement strength values.

high-strength RC beam has the same initial bending stiffness as the ordinary RC beam. When the peak overpressure of blast load exceeds point *A* (0.25 MPa), the bending stiffness of RC beam is significantly reduced due to concrete cracking in the tensile zone. In section *AB*, the blast load and displacement show a nonlinear relationship, and the bending stiffness fluctuates to a certain extent. This is because with an increase in blast load, the RC beam produces new cracks, while the initial crack continues to develop towards the beam height. After the blast load increases to point *B*, the tensile reinforcement of RC beam begins to yield and enter the hardening stage, after which the member displacement increases rapidly with the load. When the blast load exceeds *C* point, the bending failure of the three RC beams with large deformation occurs.

The protective structures subjected to explosion dynamic loads are usually allowed to work in the plastic stage, and ductility is an important index to ensure that the bending component does not undergo a sudden brittle failure. The ductility of component is usually expressed by the ductility ratio β and calculated as follows:

$$\beta = \frac{y_u}{y_e}, \tag{2}$$

where y_e is the corresponding displacement when the member yields and y_u is the failure displacement when the component is destroyed.

The cracking load, yield load, ultimate load and corresponding displacement of the three RC beams with the reinforcement ratio of 0.25% are obtained from Fig. 10, and the ductility ratio is calculated according to Eq. (2), as shown in Table 4.

It can be seen from Table 4 that the strength grade of reinforcement has little effect on the cracking load and cracking displacement of RC beams, but it can increase the yield load and ultimate load of component. Compared with ordinary RC beams, the ultimate load of HTB700 and HTB900 high-strength RC beams is increased by 36.7 and 60.0%, respectively. With an increase in longitudinal reinforcement strength, the yield displacement of RC beam increases, while the failure displacement and ductility ratio decrease. It can be judged from the damage nephograms that all failure modes of three RC beams are flexural failures.

2.4.2. Effect of Reinforcement Ratio. To study the influence of the reinforcement ratio on the RC beam resistance curve, the influence of different reinforcement ratios on the deformation characteristics and failure mode of the RC beam was analyzed. Figure 11 shows the load–displacement curves of RC beams with the reinforcement ratios increasing from 0.25 to 0.57%.

TABLE 4. Ductility and Failure Mode of RC Beams with Different Reinforcement Strength Values

RS (MPa)	CL (MPa)	CD (mm)	YL (MPa)	YD (mm)	UL (MPa)	UD (mm)	Ductility ratio	Failure mode
400	0.25	0.76	0.31	4.25	0.450	31.30	7.36	Flexural
700	0.25	0.76	0.47	8.02	0.615	29.22	3.64	Flexural
900	0.25	0.76	0.55	10.84	0.720	26.10	2.41	Flexural

Note. Here and in Table 5: RS is reinforcement strength, CL is cracking load, CD is cracking displacement, YL is yield load, YD is yield displacement, UL is the ultimate load, and UD is the ultimate displacement.
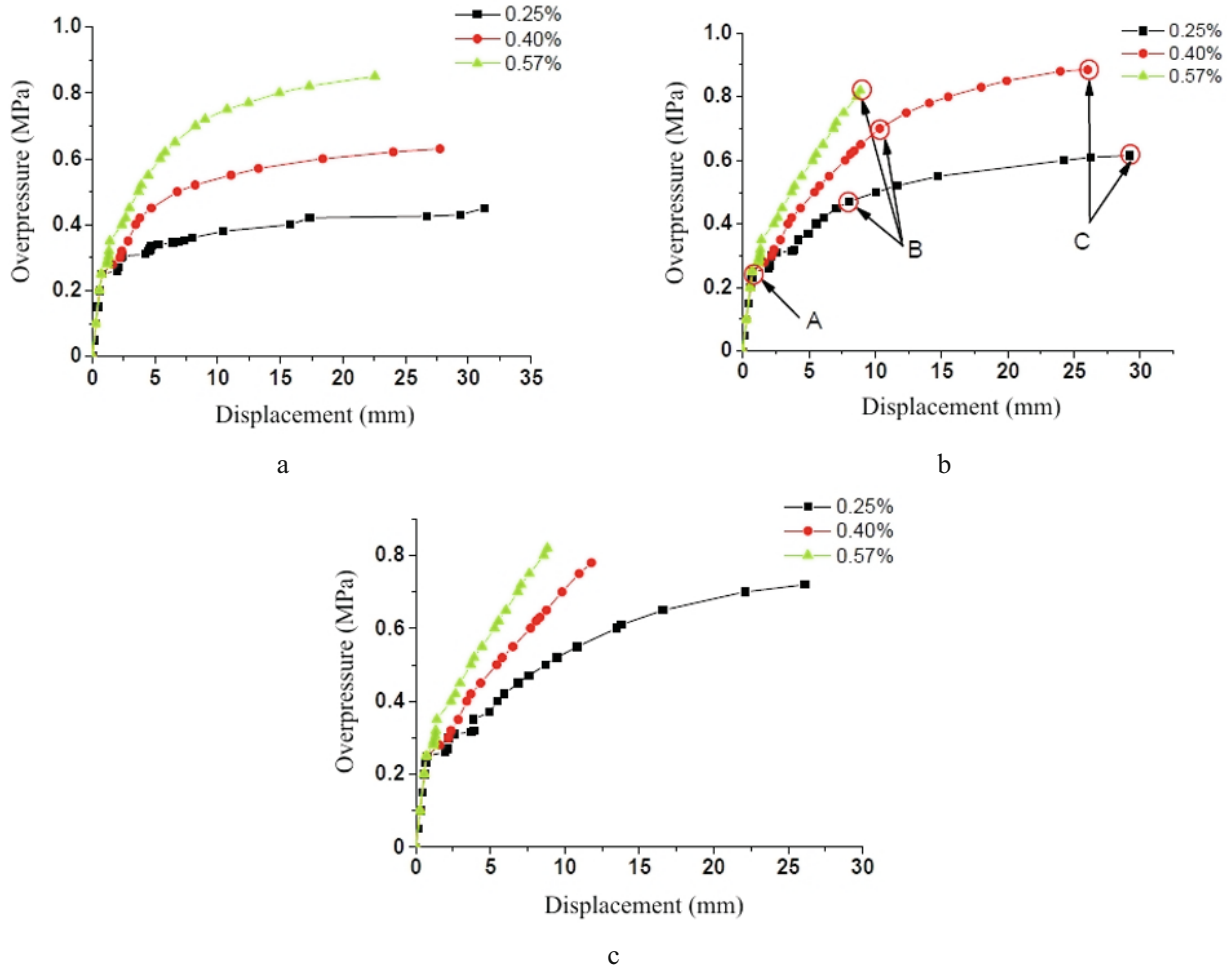

Fig. 11. Load–displacement curves of RC beams with different reinforcement ratios: (a) HRB400; (b) HTB700; (c) HTB900.

The resistance of RC beams increases with reinforcement ratio when the HRB400 is used as the main reinforcement, as shown in Fig. 11a. It can be seen from Fig. 11b that for the HTB700 high-strength RC beam, when the reinforcement ratio increases from 0.25 to 0.40%, the ultimate load of the member increases by 43.9%. However, when the reinforcement ratio increases from 0.40 to 0.57%, the ultimate load of the HTB700 high-strength RC beam is reduced by 7.3%. At this time, its resistance curve is composed only of two segments, *OA* and *AB*. When the peak overpressure of the blast load exceeds 0.82 MPa, the ultimate displacement at the mid-span section is only 8.6 mm, indicating that the RC beam has shear brittle failure. This is because the shear force at the RC beam support reaches its shear capacity. The similar phenomenon occurs in the HTB900 high-strength RC beam, as shown in Fig. 11c.

TABLE 5. Ductility and Failure Mode of RC Beams with Different Reinforcement Ratios

| RS (MPa)	RR (%)	CL (MPa)	CD (mm)	YL (MPa)	YD (mm)	UL (MPa)	UD (mm)	Ductility ratio	Failure mode
400	0.25	0.25	0.76	0.31	4.25	0.450	31.30	7.36	Flexural
	0.40	0.25	0.76	0.45	4.72	0.630	27.74	5.88	Flexural
	0.57	0.25	0.76	0.65	6.60	0.850	22.53	3.41	Flexural
700	0.25	0.25	0.76	0.47	8.02	0.615	29.22	3.64	Flexural
	0.40	0.25	0.76	0.70	10.34	0.885	26.03	2.52	Flexural
	0.57	0.25	0.76	–	–	0.820	8.86	–	Direct shear
900	0.25	0.25	0.76	0.55	10.84	0.720	26.10	2.41	Flexural
	0.40	0.25	0.76	–	–	0.780	11.79	–	Direct shear
	0.57	0.25	0.76	–	–	0.820	8.83	–	Direct shear

Note. RR is reinforcement ratio.
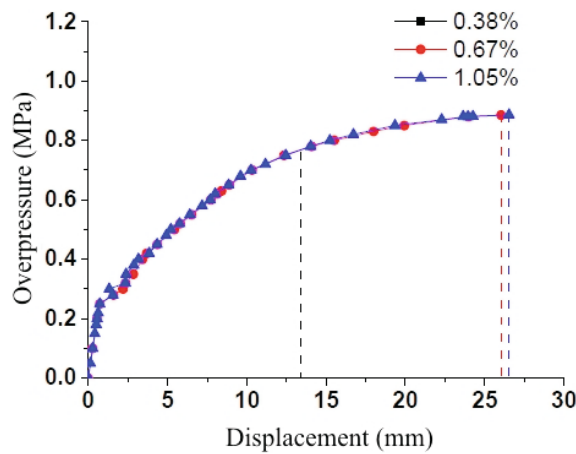
Fig. 12. Load–displacement curves of HTB700 high-strength RC beams with different stirrup ratios.

When the reinforcement ratio is increased to 0.4%, the failure mode changes. The ductility ratio and failure modes of RC beams with different reinforcement ratios are shown in Table 5.
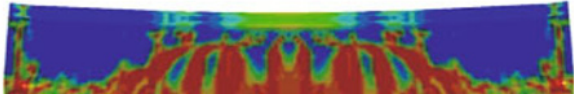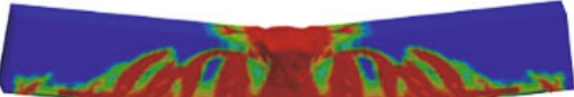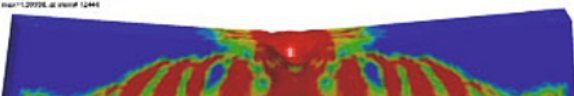
It can be seen from Table 5 that an increase in reinforcement ratio has little effect on the crack load and crack displacement of the component but can improve the yield capacity and ultimate bearing capacity. At the same time, the increase of reinforcement ratio reduces the ductility ratio of RC beams and the failure mode of RC beams changes when the reinforcement ratio increases to a certain extent under blast load.

2.4.3. Effect of Stirrup Ratio. The stirrup ratio has a direct impact on the shear capacity of RC beams. To study the effect of stirrup ratio on the resistance curve of RC beams, the effect of different stirrup ratio on the deformation and failure mode of RC beams is analyzed. Figure 12 shows the load–displacement curves of HTB700 high-strength RC beams with stirrup ratios of 0.38, 0.67, and 1.05%, respectively, when the reinforcement ratio is 0.4%.

It can be seen from Fig. 12 that the load–displacement curves of each RC beam basically coincide before the failure. With an increase in stirrup ratio, the ultimate load and corresponding displacement of RC beam increase first and then remain basically unchanged.

Analyzing concrete damage nephograms, it can be seen that the failure mode of HTB700 high-strength RC beams is a direct shear brittle failure when the stirrup ratio is 0.38%, while a typical bending failure occurs when the stirrup ratio is 0.67%. Therefore, the ultimate load and displacement of RC beams increase greatly. Thereafter, increasing the stirrup ratio has no obvious effect on improving the ultimate load and ultimate displacement of RC beam. The failure mode of RC beams is shown in Table 6.

TABLE 6. Ultimate Load and Failure Mode of HTB700 High-Strength RC Beams with Different Stirrup Ratios

Stirrup ratio (%)	Ultimate load (MPa)	Ultimate displacement (mm)	Damage nephograms	Failure mode
0.38	0.760	13.4		Direct shear
0.67	0.885	26.0		Flexural
1.05	0.886	26.5		Flexural

It can be seen from Table 6 that when the stirrup ratio increases from 0.38 to 0.67%, the ultimate load and the ultimate displacement of HTB700 high-strength RC beams increase by 16.4 and 94.0%, respectively. When the stirrup ratio increases from 0.67 to 1.05%, the ultimate load and corresponding displacement only increase by 0.1 and 1.9%, respectively. This is because the main role of stirrups is to increase the shear capacity of component with a small contribution to flexural capacity. A further increase in stirrup ratio can improve the compressive strength of the core concrete to some extent but this effect is very limited.

CONCLUSIONS

1. The anti-explosion ability of RC beams can be effectively improved by increasing the strength grade of high-strength reinforcement. Under the condition that the reinforcement and stirrup ratios are 0.25 and 0.67%, respectively, the ultimate capacity of HTB700 and HTB900 high-strength RC beams is increased by 36.7 and 60.0%, respectively, a compared to that of HRB400 ordinary RC beams.

2. Increasing the reinforcement ratio can effectively improve the anti-explosion performance of high-strength RC beams when the shear capacity is high enough. The anti-explosion performance of high-strength RC beams may decrease due to the change of its failure mode when the reinforcement ratio increases to a certain extent.

3. The shear capacity of high-strength RC beams can be improved by increasing the stirrup ratio to prevent the component from direct shear failure or bending-shear failure under high overpressure blast load. This ensures that the high flexural capacity of the high-strength RC beam is fully utilized. For high-strength RC beams with a high enough shear capacity, increasing stirrup ratio has little effect on the anti-explosion performance.

REFERENCES

1. Y. Liu, J. B. Yan, and F. L. Huang, "Behavior of reinforced concrete beams and columns subjected to blast loading," *Defence Technol.*, **14**, No. 5, 550–59 (2018).
2. C. W. Zhang, G. Gholipour, and A. A. Mousavi, "Nonlinear dynamic behavior of simply-supported RC beams subjected to combined impact-blast loading," *Eng. Struct.*, **181**, 124–142 (2019).

3. Z. P. Kuang, Q. M. Yang, and M. Cui, "Experiment research and failure modes analyses of RC-beams under blast loading," *J. Tongji University (Natural Science)*, **37**, No. 9, 1153–1156 2009).

4. W. X. Chen, H. B. Lu, X. W. Hou, and B. K. Zhou, "Tests for anti-blast performance of concrete slabs with high-strength reinforcements under blast loading," *J. Vib. Shock*, **34**, No. 10, 135–141 (2015).

5. M. S. Li, J. Li, H. Li, et al., "Deformation and failure of reinforced concrete beams under blast loading," *Expl. Shock Waves*, **35**, No. 2, 177–183 (2015).

6. S. Yao, D. Zhang, F. Y. Lu, et al., "Damage features and dynamic response of RC beams under blast," *Eng. Fail. Anal.*, **62**, 103–111 (2016).

7. D. Yoo, N. Banthia, S. Kim, and Y. Yoon, "Response of ultra-high-performance fiber-reinforced concrete beams with continuous steel reinforcement subjected to low-velocity impact loading," *Compos. Struct.*, **126**, 233–245 (2015).

8. L. Mao and S. J. Barnett, "Investigation of toughness of ultra high performance fibre reinforced concrete (UHPFRC) beam under impact loading," *Int. J. Impact Eng.*, **99**, 26–38 (2017).

9. S. D. Adhikary, B. Li, and K. Fujikake, "Dynamic behavior of reinforced concrete beams under varying rates of concentrated loading," *Int. J. Impact Eng.*, **47**, 24–28 (2012).

10. R. J. Thomas, K. Steel, and A. D. Sorensen, "Reliability analysis of circular reinforced concrete columns subject to sequential vehicular impact and blast loading," *Eng. Struct.*, **168**, 838–851 (2018).

11. T. Krauthammer and S. Astarlioglu, "Direct shear resistance models for simulating buried RC roof slabs under airblast-induced ground shock," *Eng. Struct.*, **140**, 308–316 (2017).

12. Y. Li, O. Algassem, and H. Aoude, "Response of high-strength reinforced concrete beams under shock-tube induced blast loading," *Constr. Build. Mater.*, **189**, 420–437 (2018).

13. D. G. Tang, Z. Liao, Y. L. Xue, and R. Zheng, "Research for flexural behavior of concrete beams with high-strength reinforcements under blast loading," *J. Huazhong Univ. Sci. Technol. (Natural Science Edition)*, **45**, No. 3, 122–126 (2017).

14. L. Schwer and L. J. Malvar, "Simplified concrete modeling with *MAT_CONCRETE_ DAMAGE_REL3," LS-DYNA Anwenderforum, H-I-49-60, Bamberg, Germany (2005).

15. L. J. Malvar, J. E. Crawford, and K. Morrill, *K&C Concrete Model Release 3 – Automated Generation of Material Model Input*, Technical Report TR-99-24-B1, Karagozian & Case Structural Engineers (2000).

16. L. J. Malvar, J. E. Crawford, J. W. Wesevich, and D. Simons, "A plasticity concrete material model for DYNA3D," *Int. J. Impact Eng.*, **19**, Nos. 9–10, 847–873 (1997).

17. *LS-DYNA Keyword User's Manual*, Vol. II: *Material Models*, Livermore Software Technology Corporation (LSTC), Livermore, CA (2013), pp. 18–39.

18. B. Yan, F. Liu, D. Y. Song, and Z. G. Jiang, "Numerical study on damage mechanism of RC beams under close-in blast loading," *Eng. Fail. Anal.*, **51**, 9–19 (2015).

19. T. J. Holmquist, G. R. Johnson, and W. H. Cook, "A computational constitutive model for concrete subjected to large strains, high strain rates, and high pressures," in: Proc. of the 14th Int. Symp. on Ballistics, Vol 2: *Warhead Mechanisms, Terminal Ballistics*, Quebec (1993), pp. 591–600.

20. *CEB-FIP Model Code 1990: Design Code*, Telford, London (1993).

21. J. O. Hallquist, *LS-DYNA Theory Manual*, Livermore Software Technology Corporation (LSTC), Livermore, CA (2006).

22. Q. Fang and J. C. Liu, *Underground Protective Structure* [in Chinese], China Water & Power Press, Beijing (2010).

23. Z. L. Zhou, X. B. Li, and L. Hong, *Underground Protective Engineering and Structure* [in Chinese], Central South University, China (2014).